International Journal of Nanomedicine

Dovepress
Taylor & Francis Group

Open Access Full Text Article

ORIGINAL RESEARCH

Extracellular Vesicles Derived from FGF2-Primed Astrocytes Against Mitochondrial and Synaptic Toxicities in Parkinson's Disease

Xiaomin Wen[1,2,*], Wanjun Cao[2,*], Hui Ding[2], Andi Chen[2], Zhichuan Sun[2], Yazhou Wang[2], Ye Xi[2], Shengxi Wu[2]

[1]College of Life Sciences, Northwest University, Xi'an, Shaanxi, 710069, People's Republic of China; [2]Department of Neurobiology, School of Basic Medicine, Fourth Military Medical University, Xi'an, Shaanxi, 710032, People's Republic of China

*These authors contributed equally to this work

Correspondence: Shengxi Wu; Ye Xi, Department of Neurobiology, School of Basic Medicine, Fourth Military Medical University, Xi'an, Shaanxi, 710032, People's Republic of China, Email shengxi@fmmu.edu.cn; ye.xi@fmmu.edu.cn

Purpose: Mitochondrial dysfunction associated with neuronal degeneration and subsequent synaptic disconnection are essential for the development of Parkinson's disease (PD). Considering that astrocytes play key roles in synaptogenesis during development, we hypothesized that fibroblast growth factor – 2 (FGF2), a key factor for astrocyte development, could reverse the toxic phenotype of reactive astrocytes, and the extracellular vesicles (EVs) derived from FGF2-primed astrocytes would enhance synaptogenesis in PD model. The present study was to test this hypothesis.

Methods: EVs isolated from FGF2-primed astrocytes (FGF2-EVs) were characterized by transmission electron microscopy and nanoparticle tracking analysis. FGF2-EVs were applied to both in vitro and in vivo models of PD. EVs derived from naïve astrocytes (CON-EV) were used as control. Mitochondrial alterations, neuronal survival, synaptogenesis, and mice behavior were subsequently evaluated by quantitative real-time polymerase chain reaction, Western-blotting, immunohistochemistry, and CatWalk gait analysis. To dissect the underlying mechanisms, proteomic analysis and small interfering RNA (siRNA) mediated gene silencing were adopted.

Results: FGF2 treatment restored the expression of neural progenitor markers and suppressed the levels of A1 astrocytic markers in MPP^+ pretreated astrocytes. FGF2-EVs, in comparison with that of CON-EVs, effectively protected neurons from mitochondrial fragmentation and stimulated synaptogenesis, as evidenced by expression of Mitofusin 2 (Mfn2), postsynaptic density protein 95 (PSD-95) and synaptophysin (SYP). Proteomic analysis revealed high enrichment of neural cell adhesion molecule 1 (NCAM1) in FGF2-EVs. Knocking down NCAM1 severely influenced the expression of mitochondrial and synaptic proteins. Furthermore, delivery of FGF2-EVs significantly enhanced the survival of TH+ neurons, the levels of NCAM1 and synaptogenesis in the substantia nigra of PD mice, as well as the locomotion of PD mice.

Conclusion: EVs from FGF2-primed astrocytes are superior in protecting PD mice against mitochondrial and synaptic toxicities, possibly through NCAM1, which could be used as a therapeutic strategy for PD.

Keywords: Parkinson's disease, astrocyte, extracellular vesicles, mitochondria, synaptogenesis, FGF2

Introduction

Parkinson's disease (PD) is the second most prevalent neurodegenerative diseases around the world. The primary symptoms of PD include bradykinesia, resting tremor, and muscle rigidity, which severely influence the life quality of patients.[1] The syndromes are caused by gradual degeneration of dopamine neurons in substantia nigra. Currently, the main treatments for PD are deep brain stimulation (DBS) and dopamine replacement. Both treatments can partially restore the function of local circuits and rely on the survival of residual dopamine neurons. Thus, simultaneously preventing neuronal degeneration and stimulating synaptic reconnection would produce better outcomes for PD treatment. In past decades, evidence is accumulating that mitochondrial dysfunction plays a central role in the gradual death

Received: 24 December 2024
Accepted: 7 April 2025
Published: 13 April 2025

of dopamine neurons and subsequent decline of synaptic connection. Many studies have been carried out to prevent the mitochondria dysfunction associated neuronal death.[2,3] However, few were aimed to stimulate synaptogenesis, nevertheless both.

Physiologically, astrocytes provide both neurotrophic and synaptogenic factors to neurons.[4,5] Unfortunately, a large portion of reactive astrocytes in substantia nigra switch into a neurotoxic phenotype in PD models, making the microenvironment hostile.[4,6,7] Previous studies have attempted to reprogram reactive astrocytes into dopaminergic neurons,[8,9] but these studies were seriously challenged.[10] Thus, converting the phenotype of toxic reactive astrocytes to neuroprotective and synaptogenic would be more realistic.

Considering that reactive astrocytes usually show certain "dedifferentiation" properties, we speculate that factors involved in astrocytic development would switch the phenotype of toxic reactive astrocytes to neurotrophic. Fibroblast growth factor-2 (FGF2) is a key regulator of astrocytic differentiation.[11,12] In comparison with other FGF family members, FGF2 is most effective in up-regulating glutamate transporter 1 in astrocyte, showing a robust effect in stimulating astrocytic maturation.[13] In addition, FGF2 can alleviate the symptoms of post-traumatic stress disorder (PTSD) in rats by facilitating glutamate-aspartate transporter (GLAST) function in astrocytes.[14] Therefore, FGF2 would be a good candidate for acclimating astrocytes towards beneficial phenotype.

Given that astrocytes crosstalk with neurons mainly via released factors, we focused on extracellular vesicles (EVs) which are nanoscale vesicles produced by cells and can cross biological membranes easily.[15,16] They act as miniature transporters carrying proteins, nucleic acids, lipids, etc.[17] and can be transported into brain through blood–brain barrier.[18] Recent studies have demonstrated that EVs are one of the crucial communication means between astrocytes and neurons.[19] It has been thought that astrocytes-derived EVs may be a promising treatment or drug carrier for PD. However, EVs of different sources usually exhibit varying compositional and functional characteristics, making the effects of treatment hard to be compared. Therefore, adopting the optimized EVs is of great importance for better outcome. In the present study, we evaluated the effects of EVs derived from FGF2-primed astrocytes (FGF2-EVs) on neuronal degeneration and synaptogenesis in both in vitro and in vivo models of PD. Our data demonstrated that FGF2-EVs not only rescued mitochondrial dysfunction, but also stimulated synaptogenesis of degenerating neurons, thereby providing a potential therapy for PD.

Materials and Methods

Cell Culture

The primary mouse astrocytes were isolated from the cerebral cortices from neonatal C57BL/6 mice (within 3 days of birth), cultured in DMEM/F12 (D8437, Sigma, Germany) containing 10% FBS, 1% glutamine (Sigma, Germany) and 1% penicillin–streptomycin (Gibco, USA), and grown on poly-L-lysine-coated (P6282-5MG, Sigma–Aldrich, USA) culture dishes for 14 days. The microglia-conditioned medium (MCM) treated with LPS (100 ng/mL, Sigma, Germany) or MPP^+ (100 nM, HY-W008719, MCE, USA) was collected and followed by filtration through a 0.22 filter membrane, then applied to primary astrocytes with or without FGF2 (8 ng/mL, Sino Biological, China),[20–22] EGF (50 ng/mL, peprotech, USA)[23,24] or BSA (50 ng/mL, MP Biomedicals, USA) for 24 h.

Primary mouse neurons were separated from the cerebral cortices of embryos (embryonic day 15) from pregnant C57BL/6 mice, cultured in Neurobasal media (Gibco, USA) containing 2% B27 (17504044, Gibco, USA), 1% glutamine, and 1% penicillin–streptomycin, and grown on poly-L–lysine-coated culture dishes, according to previous studies.[25] The mouse neuronal cell line (HT22 cell) was purchased from ATCC and cultured in DMEM (Gibco, USA) which was supplemented with 10% FBS (Gibco, USA). All the cells were cultivated in a humidified incubator (37°C, 5% CO_2).

Preparation of EVs

Primary astrocytes were cultured in T75 culture flask (Corning, USA) and incubated at 37°C in 5% CO_2. When the cell density reaches 70–80%, FGF2 (2 ng/mL) were added to the cell culture medium using exosome-free serum (Easyall, China) for 48 h. Then, EVs were prepared from the supernatant fluids of naïve astrocytes or FGF2-treated astrocytes by differential centrifugation. Briefly, the collected supernatant was centrifuged at 500 × *g* for 10 min, 2000 × *g* for 10 min, and 10,000 × *g* for 20 min at 4°C to remove cells and debris, and 100,000 × *g* for 70 min at 4°C through XPN-100 ultracentrifuge (Beckman

Coulter, USA). The pellet was harvested with sterile phosphate-buffered saline (PBS), then ultracentrifuged again at 100,000 × *g* for 70 min. Finally, the EV precipitate was resuspended in sterile PBS for further experiments. EVs were quantified by measuring the protein concentration via a BCA Protein Assay Kit (Thermo Fisher, USA).

Morphological Analysis of EVs by Transmission Electron Microscopy (TEM)

The 5 μL purified EVs were dropped on copper grids and incubated at RT for 5 min. Then, EVs were stained by 2% uranyl acetate at RT for 1 min. Excess liquid was removed on one side with filter paper and dried at RT for 20 min. Finally, the examination of EVs were acquired by TEM (Tecnai G2 Spirit BioTwin, FEI, the Netherlands) operated at 80 kV.

Particle Size Measurement of EVs by Nanoparticle Tracking Analysis (NTA)

The purified EVs were diluted using 1× PBS. Then, the sample was loaded into ZetaVIEW S/N 17–310 (Particle Metrix, Germany) using an injector for quantification counting of suspended particles. The data were analyzed by ZetaView 8.04.02.

Proteomic Analysis

EVs derived from naïve astrocytes (CON-EVs) and FGF2-EVs were lysed, proteolysed, subjected to high pH reversed-phase peptide fractionation, and analyzed using LC-MS/MS on an Orbitrap Fusion Lumos mass spectrometer (Thermo Fisher Scientific, MA, USA) connected to an EASY-nLC 1200 system. To establish a spectral database, the raw data were analyzed using Spectronaut X (Biognosys AG, Zurich, Switzerland) software, which was designed to search the UniProt database. Carbamidomethyl (C) was used as the fixed modification, oxidation (M) as the variable modification. Additionally, the false discovery rate (FDR) was set to 1% for both precursor ions and peptides. Similarly, data-independent acquisition (DIA) was acquired through ESI-MS (electrospray ionization tandem mass spectrometry) by the mass spectrometer. DIA data were detected by Spectronaut. The FDR threshold was set as 1% for both precursors and proteins. The proteins showing significant upregulation in FGF2–ADEVs were selected for additional functional analysis using the Gene Ontology (GO) and Kyoto Encyclopedia of Genes and Genomes (KEGG) databases.

Small Interfering RNA (siRNAs) Transfection

Small interfering RNAs targeting *NCAM1* or negative control siRNAs (50 nM, final concentration, Tsingke, China) were mixed with Lipofectamine 3000 Reagent (L3000-015, Thermo Fisher, USA) following the manufacturer's recommendations. Transfection efficiency was measured at 48 h by quantitative real-time polymerase chain reaction (qRT-PCR) and at 72 h by western-blotting.

RNA Isolation and qRT–PCR

Total RNA was extracted from cells using Trizol Reagent (Takara, Japan) and purified with chloroform and isopropyl alcohol. The complementary DNA (cDNA) was generated using a PrimeScript^{TM} RT Master Mix (RR036, Takara, Japan). Then, qRT-PCR reactions were performed using TB Green *Premix Ex Taq*^{TM} II (RR820A, Takara, Japan) by a Real-Time System (CFX96, Bio-Rad, USA). All experiments were carried out in triplicate and performed using *GAPDH* as the internal control. Relative target gene expression fold changes were calculated using the $2^{-\Delta\Delta CT}$ method. All primer sequences are listed in Table 1.

Western-Blotting

Lysates were harvested from cells or tissue in RIPA lysis buffer (P0013B, Beyotime, China) containing protease inhibitors (Roche, Switzerland) and lysed on ice for 20 min. The mouse brain tissue was grounded by a tissue homogenizer before lysis process. After assessing the concentration of total protein (BCA Protein Assay Kit, Thermo Fisher, USA), equal amounts of protein were separated through sodium dodecyl sulphate–polyacrylamide gel electrophoresis and electroblotted on a polyvinylidene fluoride membrane at 300 mA for 120–180 min on ice. After protein transfer, membranes were stained with Ponceau S solution (Cat: PS0073, Psaitong) for 1–2 min, imaged and subsequently washed with double-distilled water (ddH_2O). The membranes were blocked with 5% skim milk powder in TBST (0.1% Tween-20) for 2 h at room temperature and incubated overnight at 4°C with following antibodies: anti-Mfn2

Table 1 Primer Sequences

Primer name	Primer Sequence (5'-3')
GAPDH-F	GGTGAAGGTCGGTGTGAACG
GAPDH-R	CTCGCTCCTGGAAGATGGTG
NCAM1-F	GACACAGCCAGTCCGGGAA
NCAM1-R	GGTTTCCACTCAGAGGCGAG
H2-T23-F	GGACCGCGAATGACATAGC
H2-T23-R	GCACCTCAGGGTGACTTCAT
Iigp1-F	GGGGCAATAGCTCATTGGTA
Iigp1-R	ACCTCGAAGACATCCCCTTT
Gbp2-F	GGGGTCACTGTCTGACCACT
Gbp2-R	GGGAAACCTGGGATGAGATT
Fkbp5-F	TATGCTTATGGCTCGGCTGG
Fkbp5-R	CAGCCTTCCAGGTGGACTTT
Psmb8-F	CAGTCCTGAAGAGGCCTACG
Psmb8-R	CACTTTCACCCAACCGTCTT
Tm4sf1-F	GCCCAAGCATATTGTGGAGT
Tm4sf1-R	AGGGTAGGATGTGGCACAAG
Emp1-F	GAGACACTGGCCAGAAAAGC
Emp1-R	TAAAAGGCAAGGGAATGCAC
Ptgs2-F	GCTGTACAAGCAGTGGCAAA
Ptgs2-R	CCCCAAAGATAGCATCTGGA
Cd109-F	CACAGTCGGGAGCCCTAAAG
Cd109-R	GCAGCGATTTCGATGTCCAC
S100a10-F	CCTCTGGCTGTGGACAAAAT
S100a10-R	CTGCTCACAAGAAGCAGTGG

(1:1000, 9482, Cell Signaling Technology, USA), anti-Opa1 (1:1000, D6U6N, Cell Signaling Technology, USA), anti-Drp1 (1:1000, ab184247, Abcam, UK), anti-NCAM1 (1:10,000, 14,255-1-AP, Proteintech, China), anti-PSD95 (1:800, ab18258, Abcam, UK), anti-Synaptophysin (1:50000, ab32127, Abcam, UK), anti-β-actin (1:50000, AC026, ABclonal, China), anti-CD81 (1:1000, 27,855-1-AP, Proteintech, China), anti-CD9 (1:1000, 20,597-1-AP, Proteintech, China), anti-TSG101 (1:5000, 67,381-1-Ig, Proteintech, China), anti-Calnexin (1:5000, 10,427-2-AP, Proteintech, China), anti-Sox2 (1:500, 14–9811-82, Invitrogen, USA), anti-DRD1 (1:1000, 17,934-1-AP, Proteintech, China), anti-DRD2 (1:4000, 55,084-1-AP, Proteintech, China). After three washes with TBST, the PVDF membrane was incubated with horseradish peroxidase-conjugated goat anti-mouse/ rabbit IgG secondary antibodies (1:5000, CSA2108/CSA2115, Cohesion Bioscience, UK). Signals were detected by the ChemiDoc^{TM} XRS+ (Bio Rad, USA) and using the WesternLumaxLight^{TM} Superior (310208, ZETA, USA). The gray value of bands was quantified using Image J software.

Mitochondrial Membrane Potential and ROS Assay

All cells used for immunofluorescence staining are pre-seeded in confocal dishes (Thermo Fisher, USA). Immunofluorescence staining (MitoTracker Red and TMRE) was performed in HT22 cells and primary mouse neuronal cells for assessing mitochondrial morphology and membrane potential. The cells were incubated in Mito Tracker Red (50 nM, M7512, Invitrogen, USA) and TMRE (10 nM) which were diluted in HBSS (14065056, Gibco, USA) for 30 min at 37°C, as the manufacturer's instructions. After washing in PBS, the stained cells were used for observation. Reactive oxygen species (ROS) were detected by ROS Kit (CA1410, Solarbio, China) according to the manufacturer's instructions.

Mitochondrial Complex I and II Activity Assay

The cells were collected in the extract solution and further lysed for activity determination using Mitochondrial Complex I (NADH-CoQ Reductase) Activity Assay Kit (E-BC-K834-M, Elabscience, China) and Mitochondrial Complex II Activity Assay Kit (E-BC-K835-M, Elabscience, China) according to the manufacturer's instructions.

Immunofluorescent Staining

For cellular immunostaining, the primary neurons were fixed using 4% PFA, and incubated with anti-PSD95 (1:500, ab18258, Abcam, UK), anti-Synaptophysin (1:1000, ab32127, Abcam, UK), anti-tubulin-III (1:1000, ab78078, Abcam, UK) overnight at 4°C. Then, the appropriate fluorescent secondary antibody (Thermo Fisher, USA) was added at RT for 2 h. Fluorescence images were harvested through a FV-3000 confocal microscope (Olympus, Japan). For detection of apoptosis, TUNEL Kit (E-CK-A321, Elabscience, China) was used.

For tissue immunostaining, mouse brain tissue was immobilized in PFA overnight in 4°C after perfusion, dehydrated in sucrose for 48 h, and then for frozen section. Tissue sections were incubated with anti-TH (1:1500, T1299, Sigma-Aldrich, USA), anti-PSD95 (1:500, ab18258, Abcam, UK), anti-Synaptophysin (1:1000, ab32127, Abcam, UK) overnight at 4°C. The remaining steps were similar to cellular immunofluorescence staining.

Animals

Animal experiments were conducted in accordance with the guidelines of the Institutional Animal Care and Use Committee at the Fourth Military Medical University and adhered to the Animal Research: Reporting of In Vivo Experiments guidelines (FMMULL-20220930). C57BL/6 mice were purchased from the Laboratory Animal Center of the Fourth Military Medical University. The adult mice (6–8 weeks old) were randomly assigned to different groups and maintained on a 12:12 h light/dark cycle (lights on at 8:00 AM) before starting the experiments.

Establishment of Parkinson's Disease Model

For the in vitro model of PD, MPP^+ was used to cause damage to cells, which is a toxic metabolite of the neurotoxin MPTP.[26] Different MPP^+ concentrations were used to determine the optimal concentration for 24 h, with equal volume PBS for the control group. The MPP^+ concentration of 8 μM was used for further studies primary neurons.[27] For the in vivo model of PD, the MPTP was intraperitoneal injected into mice for one week (25 mg/kg once a day).[28,29]

Stereotactic Injection

C57BL/6 mice were anesthetized through intraperitoneal injection of pentobarbital sodium (50 mg/kg, i.p) and placed in a stereotaxic frame (RWD Life Science, China). To facilitate continuous administration, a cannula (RWD Life Science, China) was implanted into lateral ventricle (LV, mediolateral [ML]: 1.0 mm; anteroposterior [AP]: −0.3 mm; dorsoventral [DV]: −2.4 mm), FGF2-ADEVs or control EVs (10 μg per mouse) were injected at a rate of 2.5 μL/min via a pulled glass pipette and syringe pump (R642, RWD Life Science, China). A total volume of 4.5 μL was administered each day, for five consecutive days.

FGF2-EVs Labeling and Distribution in Mouse Brain

Purified EVs were labelled by PKH26 (MINI26-1KT, Sigma-Aldrich, USA) according to the manufacturer's instructions. PKH26-labeled EVs or saline were stereotactic injected to C57BL/6 mice's lateral ventricle, respectively (see "Stereotactic injection" for specific methods). At 24h after intracerebroventricular injection, brains were placed in fresh 4% PFA for fixing, transferred to 30% sucrose and then make 20 μm cryosections through the sliding microtome with a freezing plate (CM1950, Leica, Germany). Further, DAPI (D9564, Sigma-Aldrich, USA) was used to counterstain, and image acquisition was taken by a confocal microscope (FV3000, Olympus, Japan).

Gait Analysis

PD with or without EVs treatments were subjected to gait assessment using the CatWalk automated gait analysis system (Noldus Information Technology, Wageningen, the Netherlands). Mice were acclimatized to the testing environment for

at least 30 min prior to training or test. The mice were trained for at least 5 days before the formal test, allowing them to pass the test channel spontaneously and smoothly at least three times daily. Subsequently, experiments were conducted to capture the footprints. For each mouse, three consecutive, uninterrupted, and straight-running trials were selected for statistical analysis. Gait parameters, including cadence (number of steps per second), duration (total run time in seconds), and average speed (speed of the recorded run), were assessed using the CatWalk system (Noldus, Netherlands).

Statistics

Statistical analyses were conducted using GraphPad Prism 9.0 (GraphPad Software Inc., USA). Test for normal distribution was assessed using the Shapiro–Wilk test. The *t*-test was used for compare two experimental groups, while one-way analysis of variance (ANOVA) followed by Tukey's multiple comparison test was used to compare multiple experimental groups. All experimental data are represented as the mean ± standard error of the mean (SEM). Each experiment was performed at least in triplicate ($n \geq 3$). The specific numbers of replicates and statistical methods used for each analysis are described in the respective figure legends. $P < 0.05$ were considered as statistical significance.

Results

FGF2 Reverses the Toxic Phenotype of MPP^+ Pretreated Astrocytes

Reactive astrocytes are roughly grouped as neurotoxic A1 type which express complement C3 and multiple inflammatory factors, and neuroprotective A2 type which express neurotrophic factors.[22] In PD models, reactive astrocytes often display an A1-dominant phenotype.[30] We first assessed the effects of FGF2 on the MPP^+ pretreated astrocytes, in combination with LPS stimulation as positive control of A1 astrocytes. Western-blotting showed that FGF2 treatment effectively reversed the up-regulation of Sox2, a neural progenitor marker highly expressed by reactive astrocytes, in MPP^+-treated astrocytes, but not in LPS-treated astrocytes (Figure 1A and B). To test whether the effects were FGF2-specific, we stimulated astrocytes with EGF (another growth factor) and BSA (a representative of non-specific protein). Both EGF and BSA showed no significant effects on Sox2 expression (Supplementary Figure S1). In terms of A1- and A2-specific genes, FGF2 supplement significantly suppressed the expression of 3 out of the 5 A1 markers (*H2-T23, Iigp1, Gbp2*) examined in LPS pretreated astrocytes (Figure 1C). In MPP^+ pretreated astrocytes, FGF2 exhibited similar suppressive effects on these A1 markers (Figure 1D). With regard to A2-specific genes, FGF2 had no significant effects on all of the A2 markers we examined in both LPS and MPP^+ pretreated cells except for *Ptgs2* (Figure 1C and D). In line with these data, Western-blotting showed that FGF2 treatment dramatically reduced the levels of C3, the most widely adopted A1 marker, which was elevated after LPS or MPP^+ treatment (Figure 1E and F). These findings demonstrated that FGF2 is efficient in reversing the MPP^+ induced neurotoxic phenotype of astrocytes.

Characterization of EVs Derived from FGF2-Primed Astrocytes

Considering that EVs are the major means through which astrocytes communicate with neurons, we speculate that EVs from FGF2-primed astrocytes (FGF2-EVs) would have potent neuroprotective function. FGF2-EVs were isolated and examined using transmission electron microscopy (TEM), nanoparticle tracking analysis (NTA) (Figure 2A). Under TEM, FGF2-EVs exhibited a uniform, circular morphology with a bilayer structure (Figure 2B). NTA revealed that the diameter of these EVs was mainly around 139.9 nm (Figure 2C and D). To further characterize the FGF2-EVs, Western-blotting of EVs-specific markers CD81, CD9, and TSG101, as well as the negative marker Calnexin[31,32] was conducted. The results showed that the EVs markers CD81, CD9, and TSG101 were all highly expressed in FGF2-EVs, while Calnexin was barely detected in FGF2-EVs (Figure 2E). The data indicated that FGF2 treatment effectively induced EVs release from astrocytes.

FGF2-EVs Mitigate Mitochondrial and Synaptic Damage in Vitro

Since mitochondrial dysfunction represents one of the most predominant features of neuronal damage in PD,[33] we assessed the effects of FGF-EVs on neuronal mitochondrial morphology and function. In primary neurons, the lowest MPP^+ concentration that resulted in a significant reduction of mitofusin-2 (Mfn2, a key protein regulating mitochondrial dynamics

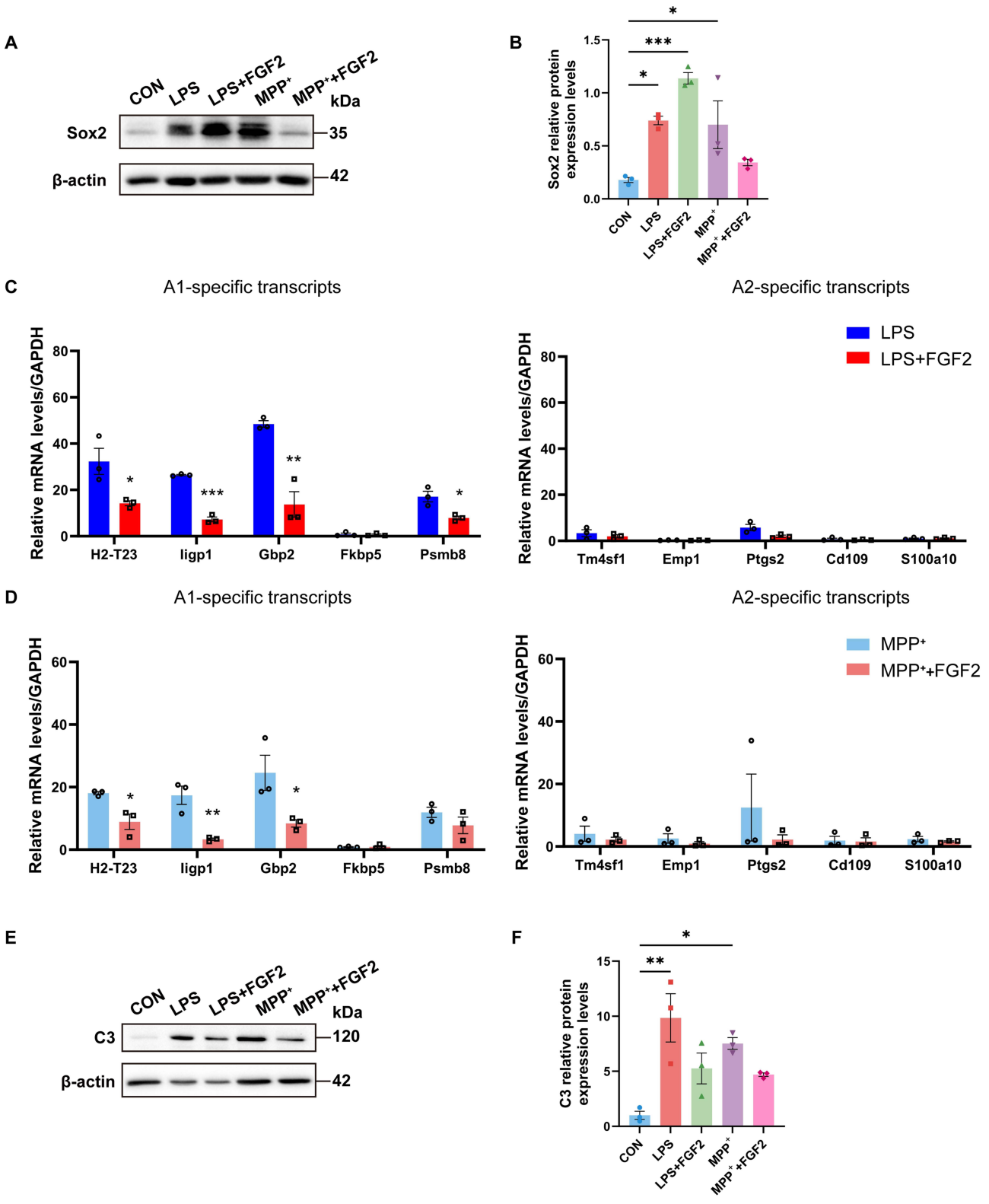

Figure 1 Effects of FGF2 on the MPP$^+$ induced "toxic" phenotype of astrocytes. (**A**) Western-blotting of Sox2 in astrocytes treated with LPS, LPS plus FGF2, MPP$^+$, MPP$^+$ plus FGF2. (**B**) Quantification of Sox2 blots in A. Notice the reversion of Sox2 expression in MPP$^+$ pretreated astrocytes by FGF2. (**C**) qRT-PCR of A1/A2 markers in astrocytes treated with LPS or LPS plus FGF2. (**D**) qRT-PCR of A1/A2 markers in astrocytes treated with MPP$^+$ or MPP$^+$ plus FGF2. (**E** and **F**) Western-blotting of C3 in astrocytes treated with LPS, LPS plus FGF2, MPP$^+$, MPP$^+$ plus FGF2, and the quantification. Notice the inhibition of A1 markers by FGF2 in both LPS and MPP$^+$ pretreated astrocytes. N = 3 batches of cells per group. Statistical analyses for B and F are performed by One-way ANOVA with Tukey's multiple comparisons test, and the analyses in (**C** and **D**) are performed by *t*-test. *P < 0.05. **P < 0.01. ***P < 0.001. Mean ± SEM.

https://doi.org/10.2147/IJN.S511474

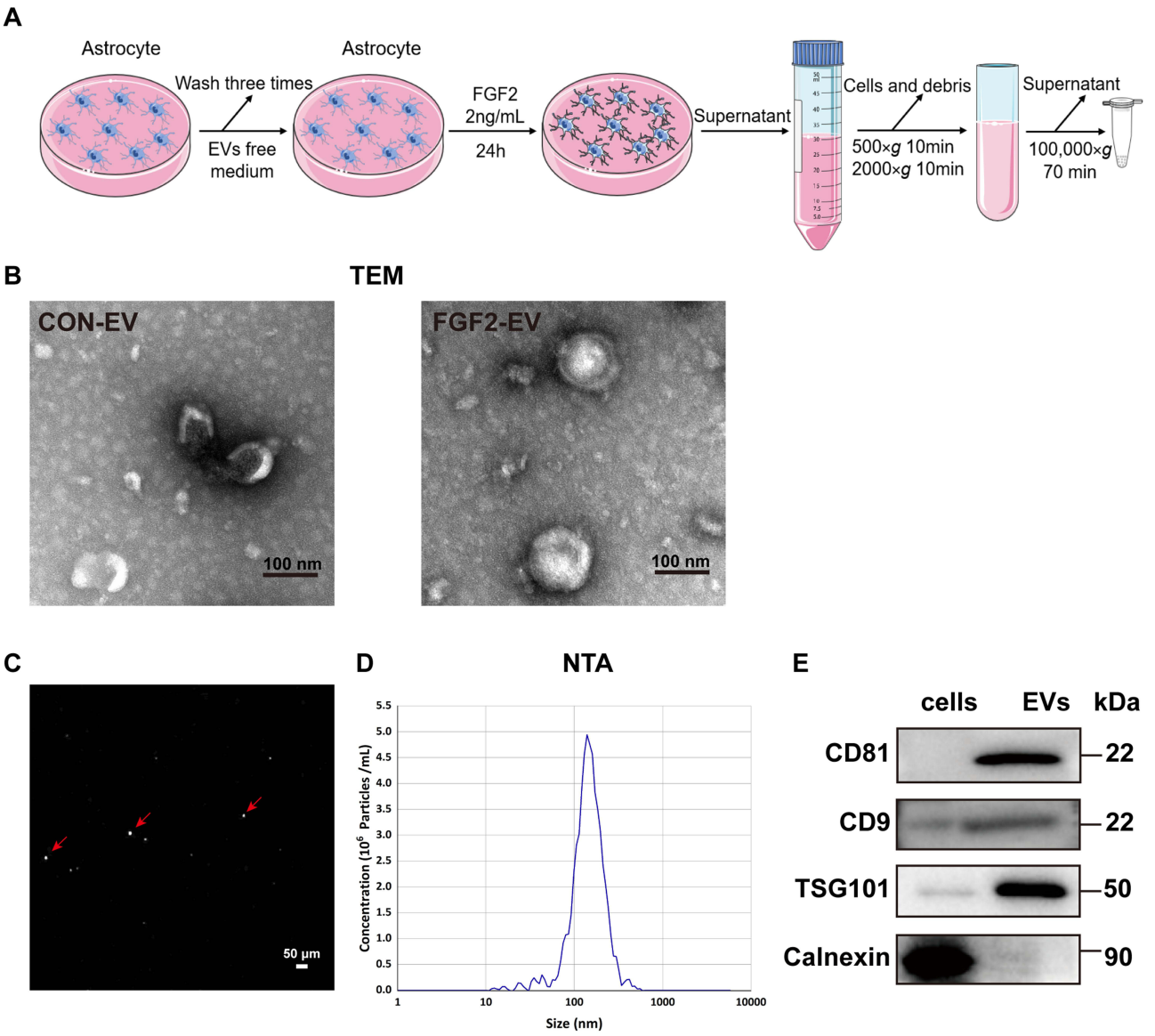

Figure 2 Preparation and characterization of EVs from FGF2-primed astrocytes (FGF2-EVs). (**A**) Schematic diagram of FGF2-EVs extraction. (**B**) Representative TEM images of CON-EVs and FGF2-EVs. (**C** and **D**) Representative images of FGF2-EVs and the particle size of FGF2-EVs as measured by NTA. Red arrows point to EVs. (**E**) Western-blotting analysis of CD81, CD9, TSG101 and Calnexin from control cells and FGF2-EVs. TEM, transmission electron microscope. NTA, nanoparticle tracking analysis.

and morphology) but not influencing cell survival (data not shown), was determined to be 8 μM (Figure 3A and B) by relative expression normalized to both β-actin and VDAC. Hence, this concentration was chosen for subsequent experiments. Compared with EVs derived from naïve astrocytes (CON-EVs), FGF2-EVs robustly increased the expression of Mfn2 which was inhibited by MPP^+ (Figure 3C and D). Analysis of MitoTracker staining showed that after MPP^+ treatment, the mitochondria of primary neurons exhibited more pronounced fragmentations, which was significantly alleviated by FGF2-EVs (Figure 3E). The aspect ratio and form factor, two crucial quantitative indices of mitochondrial fragmentation, showed obvious recovery following FGF2-EVs treatment (Figure 3F and G). Similarly, TMRE staining illustrated that FGF2-EVs reversed the MPP^+ induced suppression of mitochondrial membrane potential (Figure 3H and I). In terms of mitochondrial respiratory Complex activity, MPP^+ dramatically inhibited the activities of Complex I and Complex II, which were partially reversed by FGF2-EVs (Supplementary Figure S2). On the other hand, DCFH-DA staining revealed that FGF2-EVs dramatically reduced the generation of ROS induced by MPP^+ (Figure 3J and K). These data indicated that FGF2-EVs are efficient in alleviating MPP^+ induced mitochondrial damage.

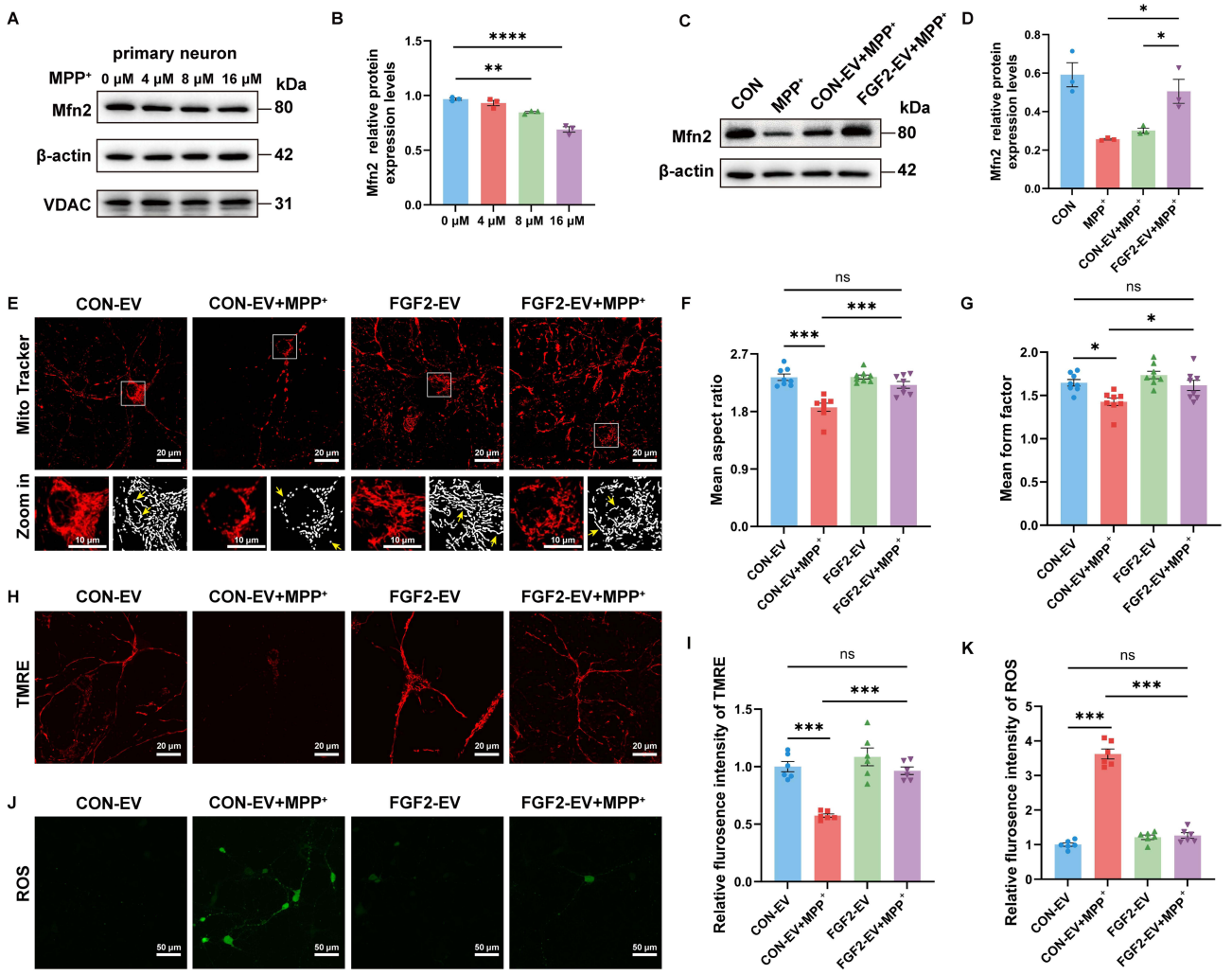

Figure 3 Effects of FGF2-EVs on the mitochondrial function of MPP^+ pretreated neurons. (**A** and **B**) Western-blotting of Mfn2 in neurons pretreated with different dose of MPP^+, and the quantification. (**C** and **D**) Western-blotting of Mfn2 in control cells, cells treated with MPP^+, MPP^+ plus CON-EVs, or MPP^+ plus FGF2-EVs, and the quantification. Notice the up-regulation of Mfn2 in FGF2-EVs treated cells. (**E**) Mito-Tracker staining of cells treated with CON-EVs, MPP^+ plus CON-EVs, MPP^+, MPP^+ plus FGF2-EVs. The yellow arrows indicate typical mitochondrial morphology in different groups. (**F** and **G**) Quantification of mitochondrial morphology. (**H** and **I**) TMRE staining and quantification of mitochondrial membrane potential (**J** and **K**) DCFH-DA staining and the quantification of ROS levels. Notice the restoration of TMRE staining and ROS levels by FGF2-EVs. N = 3 batches of cells per group in (**A**–**D**), 6 batches of cells per group in the experiment; (**E**–**K**). Statistical analyses in K for are performed by One-way ANOVA with Welch Anova multiple comparison test, and others statistical analyses are performed by One-way ANOVA with Tukey's multiple comparisons test. *P < 0.05. **P < 0.01. ***P < 0.001. ****P < 0.0001. *ns*, not significant. Mean ± SEM.

Next, we evaluated the effects of FGF-EVs on neuronal survival and synaptogenesis in the in vitro PD model. TUNEL-staining, which reflects cellular apoptosis and necrosis, showed that FGF2-EVs treatment was most effective in reducing MPP^+ induced cell death, compared with CON-EVs and FGF2 alone (Figure 4A and B). In terms of synaptic proteins, MPP^+ resulted in dramatic decrease of postsynaptic density protein 95 (PSD-95) and synaptophysin (SYP). CON-EVs did not exhibit any significant protective effects on PSD-95 and SYP (Figure 4C–F). In contrast, FGF2-EVs treatment significantly enhanced the expression of PSD-95 and SYP, to a level even higher than that of FGF2 treatment (Figure 4C–F). Interestingly, FGF2-EVs treatment resulted notable up-regulation of dopamine D1 receptor (DRD1) in cell pretreated by MPP^+ (Supplementary Figure S3). These data demonstrated that FGF2-EVs are superior in promoting neuronal survival and synaptogenesis.

Enrichment of NCAM1 in FGF2-EVs

Previous studies have shown that EVs are rich in multiple functional proteins.[34] To further elucidate how FGF2-EVs exert their functions, we performed proteomic sequencing analysis on FGF2-EVs versus CON-EVs. A total of 2308 proteins were identified in FGF2-EVs (Supplementary Table 1). Among them, 843 proteins were differentially expressed

https://doi.org/10.2147/IJN.S511474

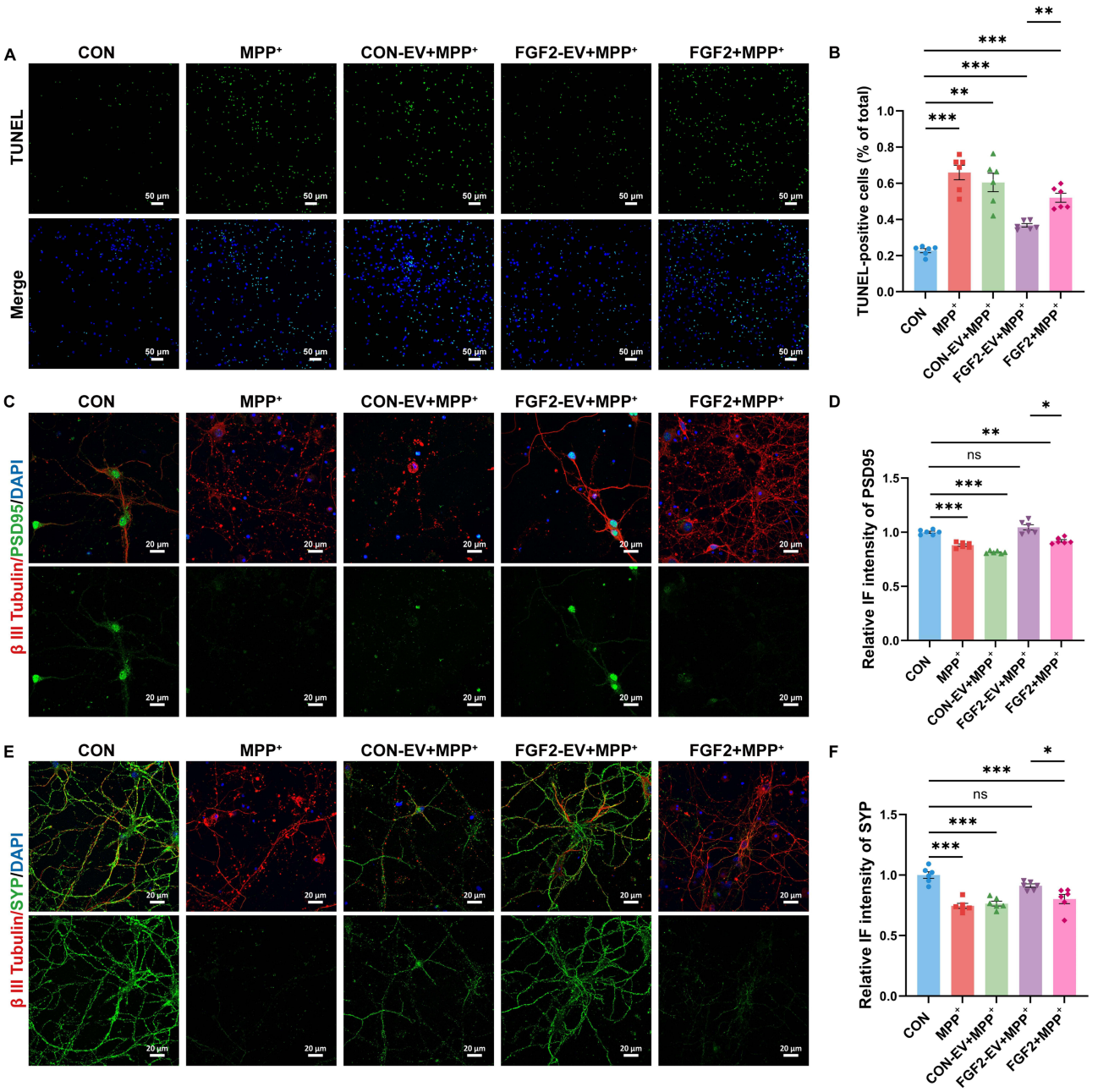

Figure 4 Effects of FGF2-EVs on the survival and synaptogenesis of MPP^+ pretreated neurons. (**A** and **B**) TUNEL staining of control neurons, neurons treated with MPP^+, MPP^+ plus CON-EVs, MPP^+ plus FGF2-EVs, MPP^+ plus FGF2, and the quantification. Notice the significant reduction of cell death by FGF2-EVs. (**C** and **D**) Double-immunostaining of β-tubulin III with PSD-95 in control neurons, neurons treated with MPP^+, MPP^+ plus CON-EVs, MPP^+ plus FGF2-EVs, MPP^+ plus FGF2, and the quantification. (**E** and **F**) Double-immunostaining of β-tubulin III with SYP in control neurons, neurons treated with MPP^+, MPP^+ plus CON-EVs, MPP^+ plus FGF2-EVs, MPP^+ plus FGF2, and the quantification. Notice the significant up-regulation of PSD-95 and SYP by FGF2-EVs. N = 6 batches of cells per group. Statistical analyses for B and D are performed by One-way ANOVA with Welch Anova multiple comparison test, and Statistical analyses for F are performed by One-way ANOVA with Tukey's multiple comparisons test. *P < 0.05. **P < 0.01. ***P < 0.001. *ns*, not significant. Mean ± SEM.

relative to CON-EVs (Figure 5A). Specifically, 306 proteins were significantly up-regulated while 537 proteins significantly down-regulated in FGF2-EVs (Figure 5B). We focused on those up-regulated proteins, among which proteins associated with cell adhesion and neurodegenerative disease were highly enriched. Venn analysis identified neural cell adhesion molecule 1 (NCAM1) as the only shared protein in these two groups of proteins (Figure 5C). NCAM1 is known as a protein closely associated with neural adhesion and neurite growth[35]. Interestingly, protein–protein interaction (PPI) analysis showed that 17 proteins in FGF2-EVs might interact with NCAM1 (Figure 5D). Among these 17 proteins, 8 were related to mitochondrial function (Figure 5E). Others were mainly related to cell adhesion,

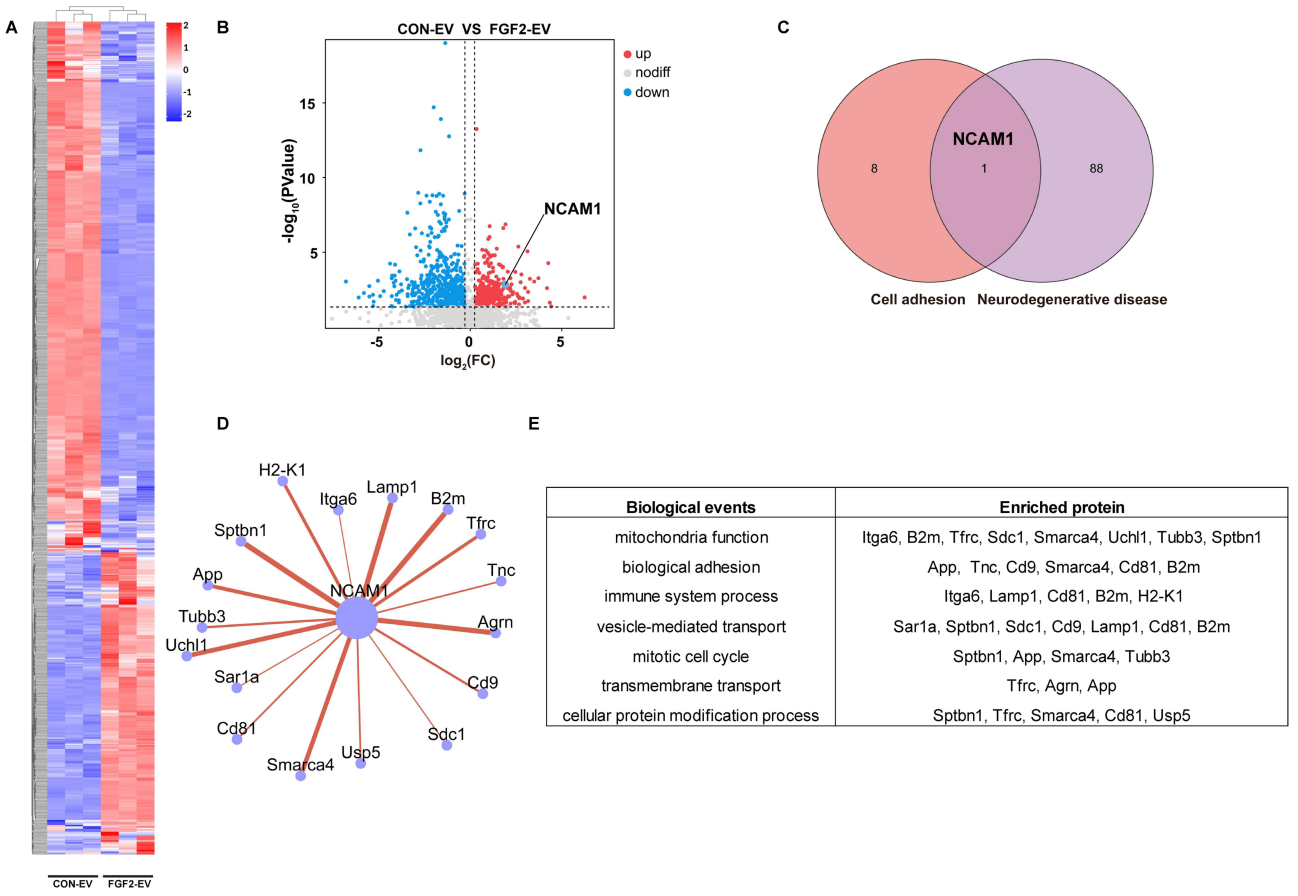

Biological events	Enriched protein
mitochondria function	Itga6, B2m, Tfrc, Sdc1, Smarca4, Uchl1, Tubb3, Sptbn1
biological adhesion	App, Tnc, Cd9, Smarca4, Cd81, B2m
immune system process	Itga6, Lamp1, Cd81, B2m, H2-K1
vesicle-mediated transport	Sar1a, Sptbn1, Sdc1, Cd9, Lamp1, Cd81, B2m
mitotic cell cycle	Sptbn1, App, Smarca4, Tubb3
transmembrane transport	Tfrc, Agrn, App
cellular protein modification process	Sptbn1, Tfrc, Smarca4, Cd81, Usp5

Figure 5 Proteomic analysis of CON-EVs and FGF2-EVs. (**A**) Hierarchical clustered heat map of differentially expressed proteins (Fold change > 1.2 and *P* value < 0.05) between FGF2-EVs and CON-EVs. Rows represent proteins and columns represent individual replicates. (**B**) Volcano plot of significantly upregulated (red dots) and downregulated (blue dots) proteins in FGF2-EVs versus CON-EVs. The location of NCAM1 was highlighted. (**C**) Venn diagram of differential proteins enriched in neurodegenerative diseases and adhesion-related differential proteins. (**D**) Protein–protein interaction network of NCAM1 in FGF2-EVs. (**E**) Functional events analysis of proteins that interact with NCAM1.

immune process, and vesicle transportation (Figure 5E), which was consistent with above observation that FGF2-EVs are efficient in regulating the inflammatory A1 astrocytes. These results indicated that FGF2-EVs are enriched with NCAM1, which may underly the beneficial effects of FGF2-EVs.

Involvement of NCAM1 in MPP$^+$-Induced Mitochondrial Damage

Previous researches have documented multiple roles of NCAM1 in the survival and development of neurons.[35,36] We next evaluated if NCAM1 were involved in the above observed beneficial effects of FGF2-EVs in vitro. MPP$^+$ treatment largely lowered the basal level of NCAM1 while FGF2-EVs treatment significantly increased the levels of NCAM1 in recipient cells (Figure 6A and B). We then adopted siRNA to knockdown the expression of NCAM1. The efficiency of si-NCAM1 was determined by Western-blotting and qRT-PCR and (Figure 6C and D, Supplementary Figure S4A–C). As expected, the knockdown of NCAM1 significantly aggravated the reduction of Mfn2 expression in the presence of MPP$^+$ (Figure 6C–E). Concurrently, the levels of Optic Atrophy 1 (Opa1) also decreased significantly, mirroring the trend of Mfn2 (Figure 6C–F). Conversely, NCAM1 knockdown enhanced the expression of Dynamin-related Protein 1 (Drp1), a critical protein for mitochondrial fission (Figure 6C–G). MitoTraker staining showed that NCAM1 knockdown exacerbated mitochondrial fragmentation, with significant decreases in aspect ratio and form factor as compared to that in MPP$^+$-treated group (Figure 6H–J). In similar, mitochondrial membrane potential, and activities of mitochondrial respiratory Complex I and II were obviously down-regulated by si-NCAM1 (Figure 6K and L, Supplementary Figure S4D–E). Additionally, DCFH-DA staining revealed further amplification of ROS production by si-NCAM1 after MPP$^+$ treatment (Figure 6M and N). Finally, TUNEL staining demonstrated that the number of apoptotic cells was significantly

https://doi.org/10.2147/IJN.S511474

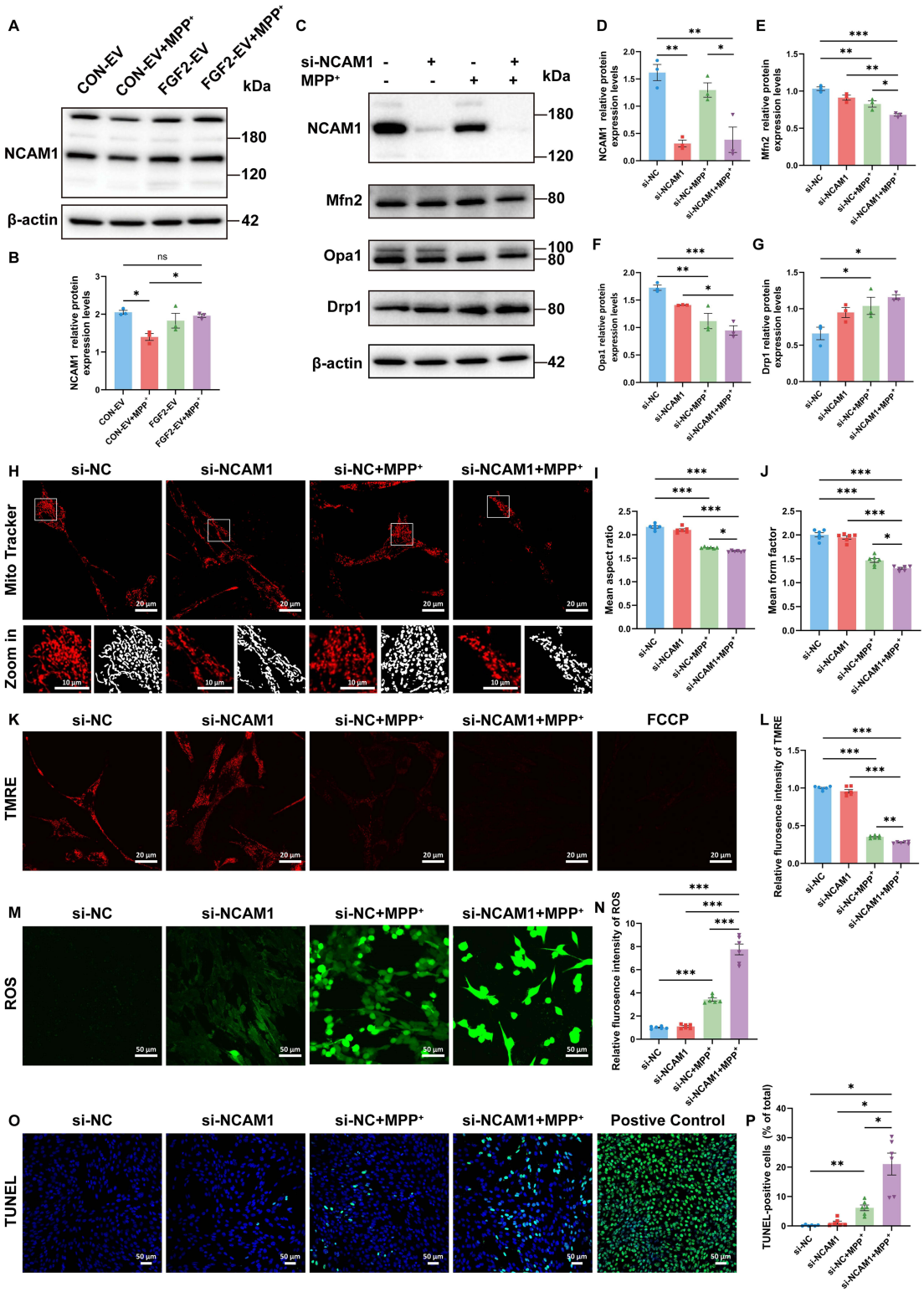

Figure 6 Effects of NCAM1 silencing on mitochondrial dynamics and function. (**A** and **B**) Western-blotting of cells treated with CON-EVs, CON-EVs plus MPP$^+$, FGF2-EVs, FGF2-EVs plus MPP$^+$, and the quantification. Notice the higher levels of NCAM1 in cells treated with FGF2-EVs. (**C–G**) Western-blotting of NCAM1, Mfn2, Opa1 and Drp1, and the quantification. si-NCAM1 decreased the expression of Mfn2 and Opa1 while increased the expression of Drp1. (**H–J**) Mito-tracker staining and corresponding measurements of aspect ratio and form factor (**K** and **L**) TMRE staining and the quantification mitochondrial membrane potential. (**M** and **N**) DCFH-DA staining and the quantification. si-NCAM1 significantly decreased fluorescent intensity of TMRE while increased that of DCFH-DA. (**O** and **P**) TUNEL staining and the quantification. si-NCAM1 significantly increased the number of TUNEL-positive cells. N = 3 batches of cells per group in (**A–G**), 6 batches of cells per group (**H–P**). Statistical analyses for N and P were performed using One-way ANOVA with Welch Anova multiple comparison test, and others statistical analyses are performed by One-way ANOVA with Tukey's multiple comparisons test. *P < 0.05. **P < 0.01. ***P < 0.001. *ns*, not significant. Mean ± SEM.

increased in the group treated with si-NCAM1 in together with MPP^+ (Figure 6O and P). Collectively, these results suggest that NCAM1 is involved in MPP^+ induced neuronal damage. FGF2-EVs would replenish NCAM1, which helps to restore mitochondrial function and against neuronal toxicity.

FGF2-EVs Up-Regulate NCAM1 and Ameliorate Mitochondrial and Synaptic Damage in PD Mice

Based on the above experiments, given the focus on developing novel strategies to mitigate PD-associated mitochondrial dysfunction, we employed the subacute MPTP-induced PD model, which has been widely recognized and validated for studying early PD pathophysiology,[37] to conduct further experiments. Specifically, we evaluated whether FGF2-EVs could exert comparable effects in MPTP-injected PD mice (Figure 7A). First, we analyzed the distribution of FGF2-EVs after lateral ventricle injection by PKH26-labeled EVs tracing. PKH26-labeled FGF2-EVs were found in multiple brain regions, with particular enrichment in substantia nigra pars compacta (SNc), cortex, and hippocampus (Figure 7B, Supplementary Figure S5). Afterward, we evaluated the effects of FGF2-EVs on the survival of dopaminergic neurons in SNc. Immunostaining of tyrosine hydroxylase (TH) showed that the number of TH-positive dopaminergic neurons was significantly increased in PD mice injected with FGF2-EVs in comparison with mice injected with CON-EVs (Figure 7C and D). Subsequently, Western-blotting analysis revealed that, in comparison with PD mice treated with control EVs, the expression level of NCAM1 was significantly enhanced in the FGF2-EVs treated mice (Figure 7E and F). In addition, the levels of Mfn2, PSD-95, and SYP exhibited similar up-regulation in FGF2-EVs treated PD mice (Figure 7E, 7G–I). Finally, CatWalk gait analysis showed that, the cadence and average speed of FGF2-EVs treated PD mice significantly increased and the duration of each step decreased, compared with those in PD mice treated with CON-EVs (Figure 7J–M). Taken together, these results suggest that FGF2-EVs can effectively mitigate dopaminergic neuronal damage in PD mice by up-regulating NCAM1 and preventing mitochondrial and synaptic dysfunction.

Discussion

Currently, most studies on PD are focused on neuronal protection, with less attention paid to synaptic reconnection. In the present study, based on the synaptogenic function of astrocytes, we first reversed the MPP^+ induced toxic phenotype of reactive astrocytes by FGF2 treatment. Then, we isolated EVs from FGF2-primed astrocytes (FGF2-EVs) and demonstrated superior beneficial effects of FGF2-EVs on mitochondrial and synaptic damage both in vitro and in vivo. Furthermore, we characterized the features of FGF2-EVs and revealed that NCAM1 mainly underlies the function of FGF2-EVs. Our data indicated that these NCAM1-enriched FGF2-EVs could be utilized as a potential therapy for PD in the future.

The development of effective therapeutics for PD still involves significant challenges. Exosomes, with their capacity to penetrate cellular barriers and features of low immunogenicity, low toxicity, and biodegradability are considered as an optimal tool for the treatment of neurodegenerative diseases.[38–40] Astrocytes, the most abundant glial cell type in the central nervous system, are capable of providing a diverse range of neuroprotection and play an indispensable role in maintaining the stability of the CNS microenvironment.[41] Naïve astrocytes can secrete EVs with neuroprotective properties.[42,43] For example, small EVs secreted by astrocytes can eliminate amyloid β-protein plaques in vivo and alleviate the toxicity of Aβ to AD neurons in *vitro*.[44] However, the contents of astrocytes vary under different circumstances,[45–47] which severely influence the outcome of EVs treatment. Hence, adopting optimized EVs from astrocyte is essential for the alleviation of PD phenotypes. In the present study, we first assessed the effects of FGF2, an important factor for the differentiation of astrocytes during development, on LPS-pretreated and MPP^+ pretreated astrocytes. The suppressive effects of FGF2 on the expression of Sox2 in MPP^+ pretreated astrocytes, not LPS-pretreated astrocytes, may reflect a direct interference of FGF2 with the intracellular alterations of MPP^+ exposure. Based on the observation that FGF2 can reverse the MPP^+ induced toxic phenotype of astrocytes, we adopted FGF2-EVs, which exhibited superior beneficial effects against mitochondrial and synaptic toxicity, as compared with CON-EVs to alleviate PD-associated neuronal damage. FGF2, by itself, has been demonstrated to be beneficial for multiple neurodegenerative diseases.[48–50] Some evidence suggests that FGF2 can enhance the survival ability of dopaminergic neurons in the substantia nigra of the 6-OHDA-induced PD mouse model.[49] FGF2 treatment likely reprograms astrocytes by altering intracellular signaling, gene expression and metabolic pathways to promote the packaging of specific bioactive cargos

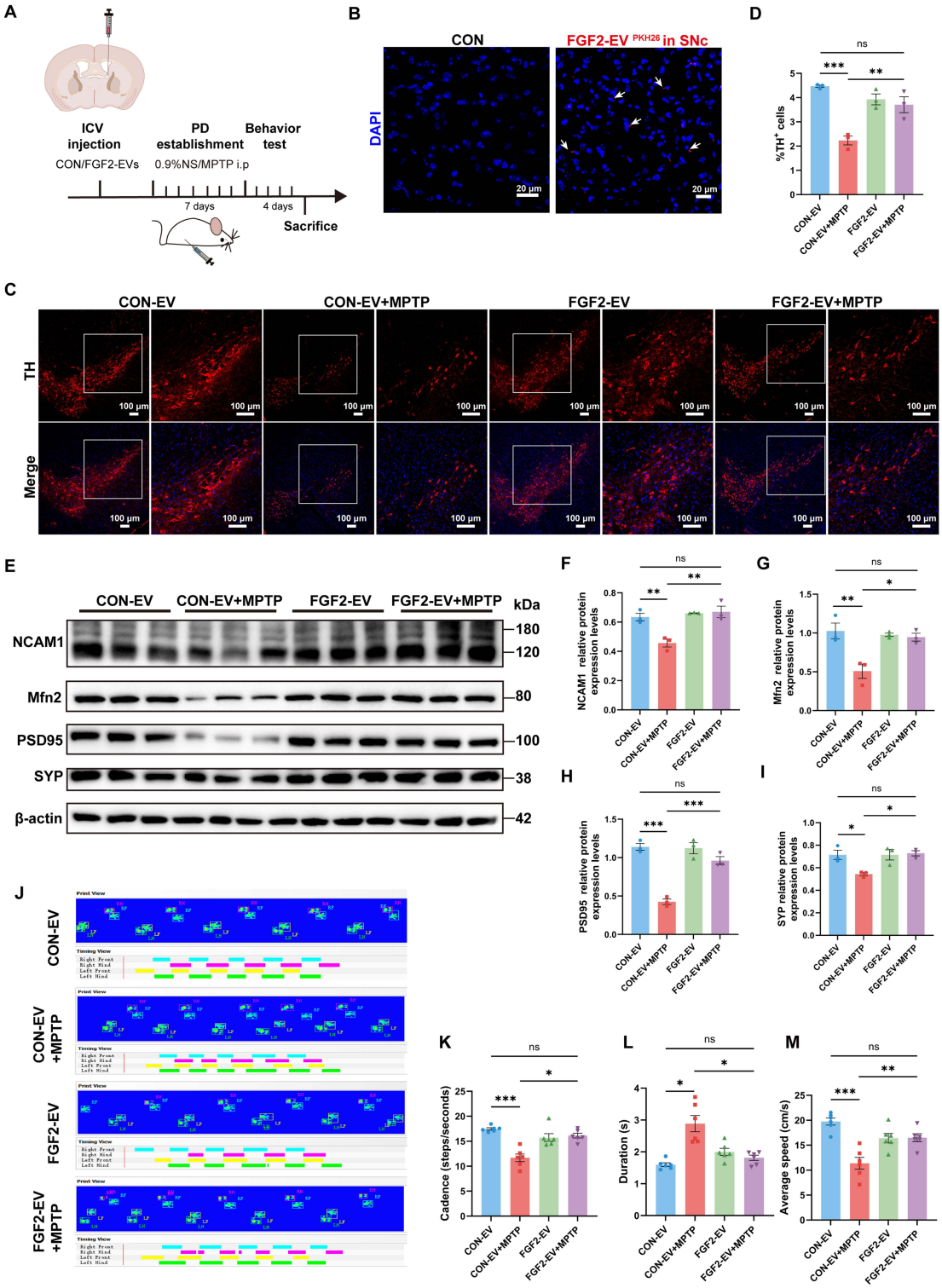

Figure 7 Effects of FGF2-EVs on the expression of NCAM1, mitochondrial and synaptic proteins, and survival of dopamine neurons in PD mice. (**A**) Experimental timeline for EVs treatment, MPTP-induced PD model establishment, and behavioral assessments. CON-EVs / FGF2-EVs were delivered to the lateral ventricle (LV) through continuous cannula. MPTP was administered to establish a PD mouse model. (**B**) Distribution of PKH26-labeled FGF2-EVs in SNc. (**C** and **D**) Immunofluorescence staining of TH and its quantification in the SNc of mice treated with CON-EVs, CON-EVs plus MPTP, FGF2-EVs, and FGF2-EVs plus MPTP. Notice the increase of the survival of dopaminergic neurons in FGF2-EVs treated PD mice. (**E**) Western-blotting of NCAM1, Mfn2, PSD95 and SYP in SNc region of mice treated with CON-EVs, CON-EVs plus MPTP, FGF2-EVs, and FGF2-EVs plus MPTP. (**F–I**) Quantitative analysis of the expression of NCAM1, Mfn2, PSD95 and SYP in Figure E. Notice the significant up-regulation of NCAM1, Mfn2, PSD95 and SYP by FGF2-EVs treatment. (**J–M**) CatWalk gait analysis of cadence, duration and average speed in mice treated with CON-EVs, CON-EVs plus MPTP, FGF2-EVs, and FGF2-EVs plus MPTP. Statistical analyses for J are performed by Kruskal–Walli's test, K are performed by One-way ANOVA with Welch Anova multiple comparison test, and others are performed by One-way ANOVA with Tukey's multiple comparisons test. N = 3 mice per group in (**B–I**), 6 mice per group in (**J–M**). *P < 0.05. **P < 0.01. ***P < 0.001. *ns*, not significant. Mean ± SEM.

into exosomes. Our data showed that FGF2-EVs are superior not only in protecting against mitochondria damage but also in stimulating synaptogenesis than FGF2 treatment. Therefore, the present study provided an optimized astrocytes-derived EVs for preventing the development of key pathological changes in PD.

In terms of glial-derived EVs, microglia-derived EVs may also be beneficial. Since the content of EVs depend on the cellular status, microglia-derived EVs may be more effective in modulating PD-associated inflammation. As the present study mainly focused on PD-associated neuronal degeneration and synaptic toxicity, we did not explore the possible effects of microglia-derived EVs under the current experimental setting.

A highlight finding of the present study, in our eyes, is the identification of NCAM1 in protecting mitochondria and stimulating synaptogenesis. Previous studies have reported that the NCAM mimetic peptide Fibroblast Growth Loop (FGL) can cross the blood–brain barrier and bind to FGF receptor (FGFR) on neurons.[51,52] NCAM can induce various neuroprotective effects via activated FGFR, thus enhancing neuronal differentiation and neurite outgrowth, facilitating synaptogenesis and long-term potentiation.[50,53] Therefore, it is reasonable that NCAM1 are enriched in FGF2-EVs. A recent study demonstrated that FGF2 enhances the release of VAMP3/cellubrevin-enriched EVs from hippocampal neurons by affecting cargo sorting.[54] We speculate that in astrocytes, FGF2 may similarly promote exosomal secretion by enriching NCAM1 cargo. What is interesting is the identification of multiple potential NCAM1-interacting proteins in EVs which are linked with mitochondrial function. Our data that si-NCAM1 severely influenced the expression of Mfn2, a protein essential for mitochondrial fusion, and ROS production, indicated a role of NCAM1 in mediating the mitochondrial protection of FGF2-EVs. Mfn2 has pleiotropic roles in cellular functions such as oxidative metabolism,[55] cell death,[56] and axonal transport in mitochondria.[57,58] Some studies have identified an involvement of Mfn2 in the pathogenesis of Charcot–Marie–Tooth disease (CMT).[59–61] In fact, NCAM1 has been regarded as a biomarker in patients and mice with progressive CMT.[62] All these are consistent with our observation that NCAM1 may play an unveiled role in regulating mitochondrial behavior or function.

In together, our data illustrated the goodness of NCAM1 enriched FGF2-EVs in against mitochondrial and synaptic toxicities of PD mice. As EVs can cross the blood–brain barrier, and FGF2-EVs can be recruited to degenerating SNc, our data indicated that these optimized EVs could be utilized for treating PD in the future.

Conclusion

Our results demonstrate that FGF2-EVs can ameliorate the injury of dopaminergic neurons in PD models by protecting mitochondrial function and stimulating synaptogenesis. The underlying mechanism may be the enrichment of NCAM1, which may interact with multiple mitochondria-related proteins (Figure 8). Further studies are worthy to be conducted to test the application of FGF2-EVs to PD treatment in clinic.

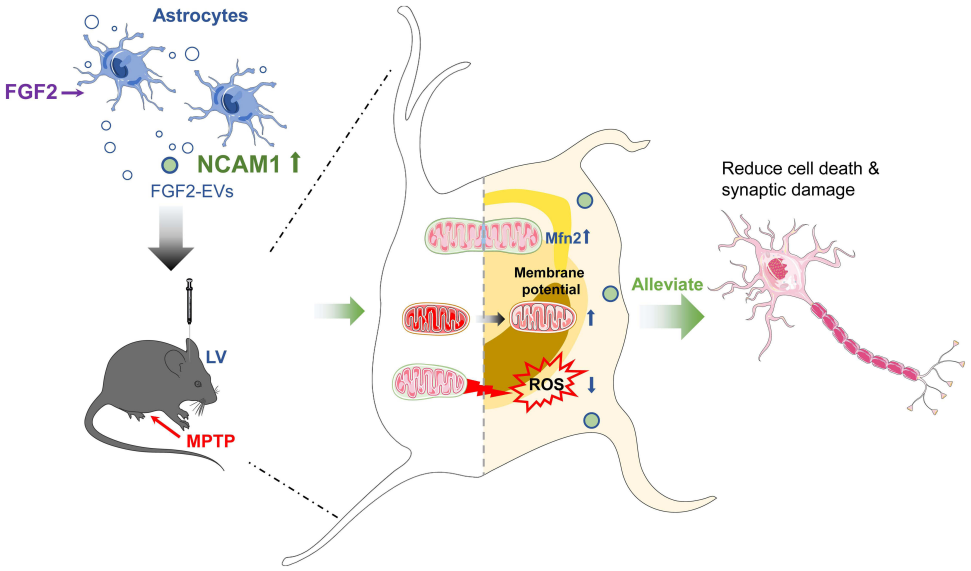

Figure 8 Graphic summary of the main finding. FGF2-EVs, which are enriched of NCAM1, are effective in alleviating the mitochondrial and synaptic impairment in PD model.

https://doi.org/10.2147/IJN.S511474

Abbreviations

CMT, Charcot–Marie–Tooth disease; DBS, deep brain stimulation; DRD1, dopamine D1 receptor; DRD2, dopamine D2 receptor; Drp1, Dynamin-related Protein 1; EVs, extracellular vesicles; FGF2, fibroblast growth factor-2; FGF2-EVs, EVs from FGF2-primed astrocytes; CON-EVs, EVs from control astrocytes; FGL, Fibroblast Growth Loop; FGFR, FGF receptor; GLAST, glutamate-aspartate transporter; LV, lateral ventricles; HIP, hippocampus; Mfn2, Mitofusin 2; MPTP, 1-methyl-4-phenyl-1,2,3,6-tetrahydropyridine; MPP^+, 1-methyl-4-phenylpyridinium; NCAM1, Neural Cell Adhesion Molecule 1; NTA, nanoparticle tracking analysis; Opa1, Optic Atrophy 1; PD, Parkinson's disease; siRNA, small interfere RNA; PTSD, post-traumatic stress disorder; qRT-PCR, quantitative real-time polymerase chain reaction; ROS, Reactive oxygen species; SNc, substantia nigra pars compacta; SYP, Synaptophysin; PSD95, Postsynaptic density protein-95; TH, tyrosine hydroxylase; TEM, transmission electron microscopy.

Data Sharing Statement

Data supporting the findings of this study are available upon request from the corresponding author.

Consent for Publication

All the authors agree to the publication of the article.

Acknowledgments

We would like to express our sincere gratitude to Prof. Dayun Feng for providing the FGF2 protein, Dr. Honghui Mao for guidance on statistical analysis and Dr. Haifeng Zhang for assistance on confocal image processing.

Author Contributions

All authors made a significant contribution to the work reported, whether that is in the conception, study design, execution, acquisition of data, analysis and interpretation, or in all these areas; took part in drafting, revising or critically reviewing the article; gave final approval of the version to be published; have agreed on the journal to which the article has been submitted; and agree to be accountable for all aspects of the work.

Funding

This study was supported by Natural Science Foundation of China (82221001 to S.W., 81901307 to Y.X.), Natural Science Basic Research Program of Shaanxi Province (2021JCW-13 to S.W., 2024JC-YBQN-0774 to Y.X.).

Disclosure

The authors report no conflicts of interest in this work.

References

1. Murakami H, Shiraishi T, Umehara T et al. Recent advances in drug therapy for Parkinson's disease. *Intern Med*. 2023;62(1):33–42. doi:10.2169/internalmedicine.8940-21
2. Moskal N, Riccio V, Bashkurov M, et al. ROCK inhibitors upregulate the neuroprotective Parkin-mediated mitophagy pathway. *Nat Commun*. 2020;11(1):88. doi:10.1038/s41467-019-13781-3
3. Han QQ, Le W. NLRP3 inflammasome-mediated neuroinflammation and related mitochondrial impairment in Parkinson's disease. *Neurosci Bull*. 2023;39(5):832–844. doi:10.1007/s12264-023-01023-y
4. Daniele S, Zappelli E, Martini C. Trazodone regulates neurotrophic/growth factors, mitogen-activated protein kinases and lactate release in human primary astrocytes. *J Neuroinflammation*. 2015;12(1):225. doi:10.1186/s12974-015-0446-x
5. Tertil M, Skupio U, Barut J, et al. Glucocorticoid receptor signaling in astrocytes is required for aversive memory formation. *Transl Psychiatry*. 2018;8(1):255. doi:10.1038/s41398-018-0300-x
6. Hwang Y, Kim HC, Shin EJ. Effect of rottlerin on astrocyte phenotype polarization after trimethyltin insult in the dentate gyrus of mice. *J Neuroinflammation*. 2022;19(1):142. doi:10.1186/s12974-022-02507-w
7. Mazzetti S, Barichella M, Giampietro F, et al. Astrocytes expressing vitamin D-activating enzyme identify Parkinson's disease. *CNS Neurosci Ther*. 2022;28(5):703–713. doi:10.1111/cns.13801
8. Guo Z, Zhang L, Wu Z et al. In vivo direct reprogramming of reactive glial cells into functional neurons after brain injury and in an Alzheimer's disease model. *Cell Stem Cell*. 2014;14(2):188–202. doi:10.1016/j.stem.2013.12.001

9. Qian H, Kang X, Hu J, et al. Reversing a model of Parkinson's disease with in situ converted nigral neurons. *Nature*. 2020;582(7813):550–556. doi:10.1038/s41586-020-2388-4
10. Wang LL, Serrano C, Zhong X et al. Revisiting astrocyte to neuron conversion with lineage tracing in vivo. *Cell*. 2021;184(21):5465–5481e5416. doi:10.1016/j.cell.2021.09.005
11. Talaverón R, Matarredona ER, Herrera A et al. Connexin43 region 266-283, via src inhibition, reduces neural progenitor cell proliferation promoted by EGF and FGF-2 and increases astrocytic differentiation. *Int J mol Sci*. 2020;21(22):8852. doi:10.3390/ijms21228852
12. Yang F, Liu Y, Tu J, et al. Activated astrocytes enhance the dopaminergic differentiation of stem cells and promote brain repair through bFGF. *Nat Commun*. 2014;5(1):5627. doi:10.1038/ncomms6627
13. Savchenko E, Teku GN, Boza-Serrano A, et al. FGF family members differentially regulate maturation and proliferation of stem cell-derived astrocytes. *Sci Rep*. 2019;9(1):9610. doi:10.1038/s41598-019-46110-1
14. Feng D, Guo B, Liu G, et al. FGF2 alleviates PTSD symptoms in rats by restoring GLAST function in astrocytes via the JAK/STAT pathway. *Eur Neuropsychopharmacol*. 2015;25(8):1287–1299. doi:10.1016/j.euroneuro.2015.04.020
15. Haney MJ, Klyachko NL, Zhao Y, et al. Exosomes as drug delivery vehicles for Parkinson's disease therapy. *J Control Release*. 2015;207:18–30. doi:10.1016/j.jconrel.2015.03.033
16. Ha D, Yang N, Nadithe V. Exosomes as therapeutic drug carriers and delivery vehicles across biological membranes: current perspectives and future challenges. *Acta Pharm Sin B*. 2016;6(4):287–296. doi:10.1016/j.apsb.2016.02.001
17. Rajendran L, Bali J, Barr MM, et al. Emerging roles of extracellular vesicles in the nervous system. *J Neurosci*. 2014;34(46):15482–15489. doi:10.1523/JNEUROSCI.3258-14.2014
18. Osaid Z, Haider M, Hamoudi R et al. Exosomes interactions with the blood-brain barrier: implications for cerebral disorders and therapeutics. *Int J mol Sci*. 2023;24(21):15635. doi:10.3390/ijms242115635
19. Upadhya R, Zingg W, Shetty S et al. Astrocyte-derived extracellular vesicles: neuroreparative properties and role in the pathogenesis of neurodegenerative disorders. *J Control Release*. 2020;323:225–239. doi:10.1016/j.jconrel.2020.04.017
20. Liu Y, Cao L, Song Y, et al. Mitochondrial glutamine transporter SLC1A5_var, a potential target to suppress astrocyte reactivity in Parkinson's disease. *Cell Death Dis*. 2022;13(11):946. doi:10.1038/s41419-022-05399-z
21. Yun SP, Kam TI, Panicker N, et al. Block of A1 astrocyte conversion by microglia is neuroprotective in models of Parkinson's disease. *Nat Med*. 2018;24(7):931–938. doi:10.1038/s41591-018-0051-5
22. Liddelow SA, Guttenplan KA, Clarke LE, et al. Neurotoxic reactive astrocytes are induced by activated microglia. *Nature*. 2017;541 (7638):481–487. doi:10.1038/nature21029
23. Linnerbauer M, Lößlein L, Vandrey O, et al. The astrocyte-produced growth factor HB-EGF limits autoimmune CNS pathology. *Nat Immunol*. 2024;25(3):432–447. doi:10.1038/s41590-024-01756-6
24. Miyatake M, Rubinstein TJ, McLennan GP et al. Inhibition of EGF-induced ERK/MAP kinase-mediated astrocyte proliferation by mu opioids: integration of G protein and beta-arrestin 2-dependent pathways. *J Neurochem*. 2009;110(2):662–674. doi:10.1111/j.1471-4159.2009.06156.x
25. Liu Z, Shen C, Li H, et al. NOD-like receptor NLRC5 promotes neuroinflammation and inhibits neuronal survival in Parkinson's disease models. *J Neuroinflammation*. 2023;20(1):96. doi:10.1186/s12974-023-02755-4
26. Blum D, Torch S, Lambeng N, et al. Molecular pathways involved in the neurotoxicity of 6-OHDA, dopamine and MPTP: contribution to the apoptotic theory in Parkinson's disease. *Prog Neurobiol*. 2001;65(2):135–172. doi:10.1016/s0301-0082(01)00003-x
27. Lavigne EG, Buttigieg D, Steinschneider R et al. Pimavanserin promotes trophic factor release and protects cultured primary dopaminergic neurons exposed to MPP+ in a GDNF-dependent manner. *ACS Chem Neurosci*. 2021;12(12):2088–2098. doi:10.1021/acschemneuro.0c00751
28. Langston JW, Ballard P, Tetrud JW et al. Chronic Parkinsonism in humans due to a product of meperidine-analog synthesis. *Science*. 1983;219 (4587):979–980. doi:10.1126/science.6823561
29. Jackson-Lewis V, Blesa J, Przedborski S. Animal models of Parkinson's disease. *Parkinsonism Related Disord*. 2012;18S183–S185 doi:10.1016/S1353-8020(11)70057-8.
30. Patani R, Hardingham GE, Liddelow SA. Functional roles of reactive astrocytes in neuroinflammation and neurodegeneration. *Nat Rev Neurol*. 2023;19(7):395–409. doi:10.1038/s41582-023-00822-1
31. Huang J, Zhang G, Li S, et al. Endothelial cell-derived exosomes boost and maintain repair-related phenotypes of Schwann cells via miR199-5p to promote nerve regeneration. *J Nanobiotechnology*. 2023;21(1):10. doi:10.1186/s12951-023-01767-9
32. Yu X, Bai Y, Han B, et al. Extracellular vesicle-mediated delivery of circDYM alleviates CUS-induced depressive-like behaviours. *J Extracell Vesicles*. 2022;11(1):e12185. doi:10.1002/jev2.12185
33. Henrich MT, Oertel WH, Surmeier DJ et al. Mitochondrial dysfunction in Parkinson's disease - a key disease hallmark with therapeutic potential. *mol Neurodegener*. 2023;18(1):83. doi:10.1186/s13024-023-00676-7
34. Colombo M, Raposo G, Théry C. Biogenesis, secretion, and intercellular interactions of exosomes and other extracellular vesicles. *Annu Rev Cell Dev Biol*. 2014;30(1):255–289. doi:10.1146/annurev-cellbio-101512-122326
35. Maness PF, Schachner M. Neural recognition molecules of the immunoglobulin superfamily: signaling transducers of axon guidance and neuronal migration. *Nat Neurosci*. 2007;10(1):19–26. doi:10.1038/nn1827
36. Zhang Y, Yeh J, Richardson PM et al. Cell adhesion molecules of the immunoglobulin superfamily in axonal regeneration and neural repair. *Restor Neurol Neurosci*. 2008;26(2–3):81–96.
37. Qi Y, Zhang Z, Li Y, et al. Whether the subacute MPTP-treated mouse is as suitable as a classic model of Parkinsonism. *Neuromolecular Med*. 2023;25(3):360–374. doi:10.1007/s12017-023-08740-7
38. Xu M, Feng T, Liu B, et al. Engineered exosomes: desirable target-tracking characteristics for cerebrovascular and neurodegenerative disease therapies. *Theranostics*. 2021;11(18):8926–8944. doi:10.7150/thno.62330
39. Rehman FU, Liu Y, Zheng M et al. Exosomes based strategies for brain drug delivery. *Biomaterials*. 2023;293:121949. doi:10.1016/j.biomaterials.2022.121949
40. Kojima R, Bojar D, Rizzi G, et al. Designer exosomes produced by implanted cells intracerebrally deliver therapeutic cargo for Parkinson's disease treatment. *Nat Commun*. 2018;9(1):1305. doi:10.1038/s41467-018-03733-8

41. Brandebura AN, Paumier A, Onur TS et al. Astrocyte contribution to dysfunction, risk and progression in neurodegenerative disorders. *Nat Rev Neurosci*. 2023;24(1):23–39. doi:10.1038/s41583-022-00641-1
42. Pascua-Maestro R, González E, Lillo C et al. Extracellular vesicles secreted by astroglial cells transport apolipoprotein D to neurons and mediate neuronal survival upon oxidative stress. *Front Cell Neurosci*. 2018;12:526. doi:10.3389/fncel.2018.00526
43. Wang G, Dinkins M, He Q, et al. Astrocytes secrete exosomes enriched with proapoptotic ceramide and prostate apoptosis response 4 (PAR-4): potential mechanism of apoptosis induction in Alzheimer disease (AD). *J Biol Chem*. 2012;287(25):21384–21395. doi:10.1074/jbc.M112.340513
44. Deng Z, Wang J, Xiao Y, et al. Ultrasound-mediated augmented exosome release from astrocytes alleviates amyloid-β-induced neurotoxicity. *Theranostics*. 2021;11(9):4351–4362. doi:10.7150/thno.52436
45. Taylor AR, Robinson MB, Gifondorwa DJ et al. Regulation of heat shock protein 70 release in astrocytes: role of signaling kinases. *Dev Neurobiol*. 2007;67(13):1815–1829. doi:10.1002/dneu.20559
46. Chun C, Smith AST, Kim H, et al. Astrocyte-derived extracellular vesicles enhance the survival and electrophysiological function of human cortical neurons in vitro. *Biomaterials*. 2021;271:120700. doi:10.1016/j.biomaterials.2021.120700
47. Wang S, Cesca F, Loers G, et al. Synapsin I is an oligomannose-carrying glycoprotein, acts as an oligomannose-binding lectin, and promotes neurite outgrowth and neuronal survival when released via glia-derived exosomes. *J Neurosci*. 2011;31(20):7275–7290. doi:10.1523/JNEUROSCI.6476-10.2011
48. Kiyota T, Ingraham KL, Jacobsen MT et al. FGF2 gene transfer restores hippocampal functions in mouse models of Alzheimer's disease and has therapeutic implications for neurocognitive disorders. *Proc Natl Acad Sci USA*. 2011;108(49):E1339–1348. doi:10.1073/pnas.1102349108
49. Timmer M, Cesnulevicius K, Winkler C, et al. Fibroblast growth factor (FGF)-2 and FGF receptor 3 are required for the development of the substantia nigra, and FGF-2 plays a crucial role for the rescue of dopaminergic neurons after 6-hydroxydopamine lesion. *J Neurosci*. 2007;27(3):459–471. doi:10.1523/JNEUROSCI.4493-06.2007
50. Woodbury ME, Ikezu T. Fibroblast growth factor-2 signaling in neurogenesis and neurodegeneration. *J Neuroimmune Pharmacol*. 2014;9(2):92–101. doi:10.1007/s11481-013-9501-5
51. Walmod PS, Kolkova K, Berezin V et al. Zippers make signals: NCAM-mediated molecular interactions and signal transduction. *Neurochem Res*. 2004;29(11):2015–2035. doi:10.1007/s11064-004-6875-z
52. Zecchini S, Bombardelli L, Decio A, et al. The adhesion molecule NCAM promotes ovarian cancer progression via FGFR signalling. *EMBO mol Med*. 2011;3(8):480–494. doi:10.1002/emmm.201100152
53. Dallérac G, Zerwas M, Novikova T, et al. The neural cell adhesion molecule-derived peptide FGL facilitates long-term plasticity in the dentate gyrus in vivo. *Learn Mem*. 2011;18(5):306–313. doi:10.1101/lm.2154311
54. Kumar R, Tang Q, Müller SA, et al. Fibroblast growth factor 2-mediated regulation of neuronal exosome release depends on VAMP3/cellubrevin in hippocampal neurons. *Adv Sci*. 2020;7(6):1902372. doi:10.1002/advs.201902372
55. Ding M, Shi R, Cheng S, et al. Mfn2-mediated mitochondrial fusion alleviates doxorubicin-induced cardiotoxicity with enhancing its anticancer activity through metabolic switch. *Redox Biol*. 2022;52:102311. doi:10.1016/j.redox.2022.102311
56. Guberman M, Dhingra R, Cross J, et al. IKKβ stabilizes mitofusin 2 and suppresses doxorubicin cardiomyopathy. *Cardiovasc Res*. 2024;120(2):164–173. doi:10.1093/cvr/cvad145
57. Macaskill AF, Rinholm JE, Twelvetrees AE, et al. Miro1 is a calcium sensor for glutamate receptor-dependent localization of mitochondria at synapses. *Neuron*. 2009;61(4):541–555. doi:10.1016/j.neuron.2009.01.030
58. Misko A, Jiang S, Wegorzewska I et al. Mitofusin 2 is necessary for transport of axonal mitochondria and interacts with the Miro/Milton complex. *J Neurosci*. 2010;30(12):4232–4240. doi:10.1523/JNEUROSCI.6248-09.2010
59. Züchner S, Mersiyanova IV, Muglia M, et al. Mutations in the mitochondrial GTPase mitofusin 2 cause Charcot-Marie-tooth neuropathy type 2A. *Nat Genet*. 2004;36(5):449–451. doi:10.1038/ng1341
60. Burté F, Carelli V, Chinnery PF et al. Disturbed mitochondrial dynamics and neurodegenerative disorders. *Nat Rev Neurol*. 2015;11(1):11–24. doi:10.1038/nrneurol.2014.228
61. Chen H, Chan DC. Mitochondrial dynamics--fusion, fission, movement, and mitophagy--in neurodegenerative diseases. *Hum mol Genet*. 2009;18(R2):R169–176. doi:10.1093/hmg/ddp326
62. Jennings MJ, Kagiava A, Vendredy L, et al. NCAM1 and GDF15 are biomarkers of Charcot-Marie-tooth disease in patients and mice. *Brain*. 2022;145(11):3999–4015. doi:10.1093/brain/awac055